Prognostic integrated image-based immune and molecular profiling in early-stage endometrial cancer

Horeweg, N.; Bruyn, M. de; Nout, R.A.; Stelloo, E.; Kedziersza, K.; Leon-Castillo, A.; ... ; Church, D.N.

Prognostic Integrated Image-Based Immune and Molecular Profiling in Early-Stage Endometrial Cancer

Nanda Horeweg[1], Marco de Bruyn[2], Remi A. Nout[1], Ellen Stelloo[3], Katarzyna Kedzierska[4], Alicia León-Castillo[3], Annechien Plat[2], Kirsten D. Mertz[5], Michelle Osse[3], Ina M. Jürgenliemk-Schulz[6], Ludy C.H.W. Lutgens[7], Jan J. Jobsen[8], Elzbieta M. van der Steen-Banasik[9], Vincent T. Smit[3], Carien L. Creutzberg[1], Tjalling Bosse[3], Hans W. Nijman[2], Viktor H. Koelzer[10,11], and David N. Church[3,12,13]

ABSTRACT

Optimum risk stratification in early-stage endometrial cancer combines clinicopathologic factors and the molecular endometrial cancer classification defined by The Cancer Genome Atlas (TCGA). It is unclear whether analysis of intratumoral immune infiltrate improves this. We developed a machine-learning, image-based algorithm to quantify density of $CD8^+$ and $CD103^+$ immune cells in tumor epithelium and stroma in 695 stage I endometrioid endometrial cancers from the PORTEC-1 and -2 trials. The relationship between immune cell density and clinicopathologic/molecular factors was analyzed by hierarchical clustering and multiple regression. The prognostic value of immune infiltrate by cell type and location was analyzed by univariable and multivariable Cox regression, incorporating the molecular endometrial cancer classification. Tumor-infiltrating immune cell density varied substantially between cases, and more modestly by immune cell type and location. Clustering revealed three groups with high, intermediate, and low densities, with highly significant variation in the proportion of molecular endometrial cancer subgroups between them. Univariable analysis revealed intraepithelial $CD8^+$ cell density as the strongest predictor of endometrial cancer recurrence; multivariable analysis confirmed this was independent of pathologic factors and molecular subgroup. Exploratory analysis suggested this association was not uniform across molecular subgroups, but greatest in tumors with mutant p53 and absent in DNA mismatch repair–deficient cancers. Thus, this work identified that quantification of intraepithelial $CD8^+$ cells improved upon the prognostic utility of the molecular endometrial cancer classification in early-stage endometrial cancer.

Introduction

Endometrial cancer is the most common gynecologic malignancy in developed countries (1, 2). Most cases are detected at early stage with disease confined to the uterus (FIGO stage I) and are managed by curative-intent surgical resection (3). Adjuvant external beam radiotherapy or vaginal vault brachytherapy reduce the risk of pelvic recurrence, but at the expense of added toxicities (3–5). Adjuvant chemoradiotherapy reduces recurrence and improves survival in high-risk cases (6). The definition of risk groups, and thus, the selection of which women should receive adjuvant local or systemic therapies has traditionally been based on clinical and pathologic factors, including patient age, stage, histologic type and grade, lymphovascular space invasion (LVSI), and myometrial invasion (7–9). However, the usefulness of several of these factors in early-stage endometrioid endometrial cancer is limited by their relatively modest effect size (9–11), resulting in considerable over- and undertreatment. This shortcoming has motivated intense investigation for novel endometrial cancer subgroups or tumor-associated biomarkers of prognostic value, using established and emerging technologies (12–15). Arguably, the most impactful of these studies is that by The Cancer Genome Atlas (14). This used whole-exome sequencing to define four endometrial cancer subgroups with differing biology and clinical outcome: (i) POLE ultramutated (POLEmut), defined by pathogenic mutations within the DNA polymerase epsilon catalytic subunit (*POLE*) exonuclease domain; (ii) DNA mismatch repair deficient (MMRd); (iii) TP53 mutant/somatic copy number alteration (SCNA) high; and (iv) an SCNA-low group lacking these other genomic alterations, and often referred to as no specific molecular profile (NSMP). Approximation of this molecular classification using surrogate markers is feasible in clinical practice (16) and improves upon prognostication provided by

[1]Department of Radiation Oncology, Leiden University Medical Center, Leiden, the Netherlands. [2]Department of Gynaecologic Oncology, University Medical Center Groningen, Groningen, the Netherlands. [3]Department of Pathology, Leiden University Medical Center, Leiden, the Netherlands. [4]Wellcome Centre for Human Genetics, University of Oxford, Roosevelt Drive, Oxford, United Kingdom. [5]Cantonal Hospital Baselland, Institute of Pathology, Liestal, Switzerland. [6]Department of Radiation Oncology, University Medical Center Utrecht, Utrecht, the Netherlands. [7]Maastricht Radiation Oncology Clinic, Maastricht, the Netherlands. [8]Department of Radiotherapy, Medisch Spectrum Twente, Enschede, the Netherlands. [9]Radiotherapiegroep, Arnhem, the Netherlands. [10]Department of Pathology and Molecular Pathology, University of Zurich, Zurich, Switzerland. [11]Department of Oncology and Nuffield Department of Medicine, University of Oxford, Oxford, United Kingdom. [12]Oxford Cancer Centre, Churchill Hospital, Oxford University Hospitals NHS Foundation Trust, Oxford, United Kingdom. [13]Oxford NIHR Comprehensive Biomedical Research Centre, Oxford University Hospitals NHS Foundation Trust, Oxford, United Kingdom.

Note: Supplementary data for this article are available at Cancer Immunology Research Online (http://cancerimmunolres.aacrjournals.org/).

Current address for R.A. Nout: Department of Radiation Oncology, Erasmus MC Cancer Institute, Rotterdam, the Netherlands.

N. Horeweg and M. de Bruyn contributed equally to this article. V.H. Koelzer and D.N. Church contributed equally as co-senior authors of this article.

Corresponding Author: David N. Church, University of Oxford, Roosevelt Drive, Oxford OX37BN, United Kingdom. Phone: 4477-0947-0345; Fax: 4418-6528-7501; E-mail: dchurch@well.ox.ac.uk

Cancer Immunol Res 2020;8:1508–19

doi: 10.1158/2326-6066.CIR-20-0149

clinicopathologic factors (11). Prospective evaluation of this classification, together with other promising molecular markers such as *CTNNB1* mutation (10, 17), is underway in both clinical trial (18) and nonclinical trial settings. Another important area of endometrial cancer biomarker research pertains to the antitumor T-cell response, the prognostic value of which has been shown in several studies (19, 20). While the potential clinical utility of both the molecular endometrial cancer classification and quantification of the antitumor immune response appear considerable, the variable prognosis of molecular endometrial cancer subgroups may be explained by a marked variation in intratumoral T-cell infiltrate between them (21, 22), and it is unclear whether these genomic and immune biomarkers confer independent prognostic value. An analysis of an endometrial cancer cohort of mixed stages and histotypes demonstrated that while application of the molecular classification improves upon the prognostication provided by clinicopathologic variables, the additional analysis of T-cell infiltrate conferred no further benefit (23). Here, we examined this in a more homogenous population of stage I endometrioid endometrial cancers from two large randomized clinical trials.

Materials and Methods

Design and study population

The design and results of both the PORTEC-1 and PORTEC-2 randomized trials have been published previously (3, 4). The PORTEC-1 trial recruited 714 patients with stage I endometrial carcinoma, grade 1 or 2 with deep (>50% thickness) myometrial invasion, or grade 2 or 3 with superficial invasion between 1990 and 1997. The PORTEC-2 trial recruited 427 patients with endometrial carcinoma with high-intermediate risk features, defined as either: (i) FIGO 1988 stage 1B (<50% myometrial invasion) with age greater than 60 and grade 3; (ii) FIGO 1988 stage 1C (≥50% myometrial invasion) with age greater than 60 and grade 1 or 2; and (iii) FIGO 1988 stage IIA (endocervical glandular involvement) with any age (except for grade 3 with deep invasion) from 2000 to 2006. Confirmation of eligibility and randomization in the PORTEC-1 and PORTEC-2 trials were done on the basis of the original pathology diagnosis. The trial protocols were approved by the Dutch Cancer Society and the medical ethics committees at participating centers; all patients provided informed consent. Long-term follow-up is available for both studies and has been published (5, 24). Cases were selected for this study based on the availability of tumor material for determination of molecular endometrial cancer subgroups, and tissue microarrays (TMA) for quantification of immune infiltrate. The study CONSORT diagram is provided in Supplementary Fig. S1.

Clinicopathologic variables and central pathology review

Demographic variables and outcomes were obtained from the trial databases. Pathologic analyses including criteria used to define LVSI and myometrial invasion were based on the results of central review (9, 11), which was performed because previous studies had poor reproducibility of tumor grading (4, 25). To undertake this, formalin-fixed paraffin-embedded (FFPE) tumor material was collected. Representative histologic slides and/or tumor samples were available from 926 (81.2%) patients with endometrioid type tumors, of the total 1,141 randomized patients (9). For both studies, specialized gynecopathologists reassessed histologic type, stage, grade, and LVSI (9, 11). At review, criteria for high-intermediate risk could be confirmed, or patients could be either reclassified to high-risk (nonendometrioid type carcinoma, IC grade 3, or stage IIB or higher), or low-risk groups. Of the 711 patients with tumor material available for quantification of immune infiltrate, 4 patients (0.6%) had tumors staged as more than stage IB on central review. In two patients, the local pathology assessment was corrected (from stage IB to stage IIIA; FIGO 2009 classification) after the patients had been included and randomized: one for implantation metastases at the tuba, and the other for tumor invasion of the serosa. The two other patients were upstaged for microscopic invasion of the cervical stroma (from stage IA to II according to the FIGO 2009 classification). As these four patients all remained in the (PORTEC-2) trial and were treated as randomized, we did not exclude them from this analysis. However, 16 cases (2.3%) that were identified as nonendometrioid endometrial cancer (NEEC) by central review were excluded from the study given the poor prognosis of this histotype.

Determination of molecular subgroups and other molecular factors

Methods used to classify cases analogous to the TCGA have been reported previously (11, 26, 27). *POLE* mutational analysis and IHC for mismatch repair (MMR) and p53 status were used to classify cases analogous to the TCGA subgroups; details of primers and antibodies have been reported previously (11, 26, 27). Pathogenic *POLE* mutations were detected by sequencing *POLE* hotspot exons (26). MMR status was determined by IHC in all cases; tumors were categorized as MMRd if tumor cells showed loss of nuclear staining of at least one of the mismatch repair proteins, and MSS if tumor cells showed nuclear positivity for all mismatch repair proteins. p53 status was classified as mutant (p53-mutant) if >50% of the tumor cells showed a strong positive nuclear staining, or when discrete geographical patterns showed >50% tumor cell positivity. Tumors in which no tumor p53 staining was observed were sequenced for exon 5–8 *TP53* mutations. Tumors with normal p53 staining were classified as p53 wild type. L1 cell adhesion molecule (L1CAM) positivity was defined as ≥10% positive cells, as published previously (11). *CTNNB1* mutation status was determined by next-generation sequencing (NGS) of exon 3. Cases with more than one classifying feature (e.g., *POLE* mutation and p53-mutant immunostaining pattern) were classified according to the dominant molecular feature on the basis of pathogenicity (e.g., MMRd cases with nonpathogenic *POLE* mutations were assigned to MMRd classifier; ref. 28; Supplementary Table S1). MMRp cases lacking pathogenic *POLE* mutation or p53 abnormality/mutation were assigned to the NSMP category. Methods used to determine additional molecular factors have been reported previously (11, 15)

CD8 and CD103 immunostaining

TMAs of the PORTEC-1 and PORTEC-2 trials were produced as described previously (3, 4) Dual-marker IHC was performed using a modification of a previously published protocol (29) as follows. FFPE slides were deparaffinized and rehydrated in graded ethanol. Antigen retrieval was initiated with a preheated 10 mmol/L citrate buffer (pH = 6) and endogenous peroxidase activity was blocked by submerging sections in a 0.45% hydrogen peroxide solution. Slides were blocked in PBS containing 1% human serum and 1% BSA. Slides were incubated overnight with rabbit anti-human CD103 (1 mg/L; anti-E7-integrin, clone ERPR4166(2), catalog number Ab129202, Abcam) at 4°C. Subsequently, slides were incubated with a ready-to-use peroxidase-labeled polymer for 30 minutes (Envision+/HRP anti-mouse, catalog number K4001, Dako). Signal was visualized with StayYellow/HRP (catalog number Ab169561, Abcam) solution according to the manufacturer's instructions. Slides were incubated overnight with mouse anti-human CD8 (3 mg/L, clone C8/144B,

catalog number GA62361–2, DAKO, Agilent Technologies) at 4°C. Subsequently, slides were incubated with a ready-to-use alkaline phosphatase-labeled polymer for 30 minutes (ImmPRESS-AP Anti-Mouse IgG Polymer Detection Kit, catalog number MP-5402–50, VECTOR laboratories). Signal was visualized with Fast Red Substrate Kit (catalog number Ab64254, Abcam) solution according to the manufacturer's instructions and slides were counterstained with hematoxylin. Appropriate washing steps with PBS were performed in between incubation steps. Sections were embedded in Eukitt mounting medium (Sigma Aldrich). Satisfactory immunostaining was confirmed by visual inspection of control samples (colon, secretory endometrium, proliferative endometrium, vulva, placenta, and tonsil) from scanned images acquired by a Hamamatsu slide scanner (Hamamatsu photonics).

Machine learning–based quantification and localization of immune infiltrate

TMAs were produced as previously described (27). Dual marker for CD8 and CD103 was performed on TMA sections cut at 4 μm using a modification of a previously reported protocol (29). Slides were scanned at high resolution (×200) using an Aperio slide scanner (Leica Biosystems). TMA cores were segmented using the HALO digital image analysis software version v3.0.311.167 (Indica Labs). Digital slide review and quality control was performed by an experienced pathologist (Viktor H. Koelzer, University of Zurich, Zurich, Switzerland); spots with staining artefacts, folds or less than 1,000 cells/spot were excluded from analysis. A deep neural network algorithm (Simonyan and Zisserman VGG, HALO AI) was trained using pathologist annotated regions, to localize and quantify tumor epithelial tissue and tumor-associated stroma regions and to exclude areas of necrosis, erythrocyte aggregates, and glass background. Tissue mark-up images were generated, and classification accuracy was confirmed through pathology review. Color deconvolution was performed for detection of nuclei (hematoxylin, RGB 0.644,0.716,0.267) and the reaction product for CD8 (alkaline phosphatase, RGB 0.1,0.877,0.377) and CD103 (StayYellow/HRP, RGB 0.112,0.1,0.445). Thresholds for positive staining were set using unstained epithelium and stromal fibroblasts as internal negative controls. Marker-positive cells in stromal and epithelial regions were classified into groups according to the combination of marker positivity and quantified in each area at single-cell resolution. A total of 1,787 cores were included in the final dataset. For each spot, the total area of each tissue region, the absolute and percentage number of marker-positive cells, infiltration density (marker-positive cells/mm^2; ref. 30), cell morphometric parameters, and staining intensity were recorded. Marker densities for each case were then calculated as the mean of the densities across all cores for that case.

Concordance of pathologist estimation of tumor CD8$^+$ cell infiltrate with artificial intelligence–based quantification

Analysis of concordance between artificial intelligence (AI)–based quantification and expert pathologist review was performed in a subset of 100 cases, and was calculated for total CD8$^+$ cell counts in preference to densities, given the difficulty in accurately measuring surface area of tumor and stromal by visual inspection on the micrometer scale. To do this, we developed a practical and fast categorical scoring system with distinct cutoffs to categorize cases according to the total number of CD8$^+$ cells per TMA core, the value of which was strongly correlated with intraepithelial CD8$^+$ cell density (Spearman $\rho = 0.89$; $P < 0.001$). The AI-based quantification of this metric across all TMA cores was used to determine its quartiles (0–2, 2–16.5, 16.5–60, 60–1509), which were in turn used to define cutoff points suitable for pathologist estimation (0–5, 5–15, 15–50, and >50 CD8$^+$ cells per TMA core). Given the inability of pathologists to count cells in routine daily diagnostic practice, we asked each pathologist to categorize each case from a subset of 100 cases into one of the four groups based on visual assessment of the number of intraepithelial CD8$^+$ cells per field at low to moderate magnification and to count cells only if categorization at low power remained unclear. All analyses were done blinded to both the results of the other pathologists and to the AI-based estimate. Discordant cases were reviewed by all three pathologists to generate a consensus pathologic categorization. Both the individual pathologist and consensus categorization were tested for concordance with the AI-based estimate.

Statistical analysis

Continuous variables were analyzed by either parametric or nonparametric methods depending on their distribution. Categorical variables were analyzed by nonparametric methods. Clustering of cases according to density of immune cell infiltrate was done by hierarchical clustering using Ward minimum variance method (31, 32), with cluster number chosen based on the gap statistic (31). Biomarker analyses were performed in accordance with the REMARK guidelines (33) and are listed in Supplementary Table S2. For the analysis of immune infiltrate with clinical outcome, our primary endpoint was time to endometrial cancer recurrence defined as the time from randomization to relapse, with censoring at last contact or death in case of no recurrence. The secondary endpoint was cancer-specific survival (CSS), defined as the time from randomization to endometrial cancer death, with censoring at date of last contact or non-cancer death. Exploratory analyses are explicitly referred to as such. Survival curves were plotted using the Kaplan–Meier method, and median follow-up calculated by the reverse Kaplan–Meier method. Time-to-event analyses were performed by pooled univariable and multivariable Cox proportional hazards models, stratified by trial. Continuous marker densities were $\log_2$ transformed prior inclusion in Cox proportional hazards models. Covariables for inclusion in multivariable models were prespecified based on proven prognostic importance (11, 34), with number chosen to minimize risk of overfitting (33, 35). Multivariable models used all informative cases and excluded those with missing covariable data (maximum 4.9% of cases for any single covariable). Model validation was performed by analysis of discrimination and indices of optimism determined by means of model fitting to 1000 bootstrap resamples (35). Proportionality of hazards was confirmed by inspection of scaled Schoenfeld residuals. Sensitivity analyses to exclude confounding of study results by postoperative treatment (external beam radiotherapy or vaginal vault brachytherapy), were performed by forced-entry of a postoperative treatment variable into multivariable model, both excluding and including a intraepithelial total CD8$^+$ density*treatment interaction term. Concordance between categorization by pathologist review and AI-based quantification was calculated by weighted Cohen kappa. All P values were two-sided. Statistical significance was accepted at $P < 0.05$. Statistical analyses were performed using SPSS (Version 26) or R Version 3.6.1. (http://www.r-project.org/). R packages used in this study included:

RMS: https://cran.r-project.org/web/packages/rms/index.html
Survival: https://cran.r-project.org/web/packages/survival/index.html
ggPlot2: https://cran.r-project.org/web/packages/ggplot2/index.html
Survminer: https://cran.r-project.org/web/packages/survminer/index.html
ComplexHeatmap: https://bioconductor.org/packages/release/bioc/html/ComplexHeatmap.html

Ethical approval

The PORTEC study protocols were approved by the Dutch Cancer Society and by the medical ethics committees at participating centers. Both studies were conducted in accordance with the principles of the Declaration of Helsinki. All patients provided signed informed consent to study participation.

Results

Patient characteristics

The CONSORT diagram for this study is provided as Supplementary Fig. S1, and characteristics of included patients are shown in **Table 1**. After exclusion of cases lacking tumor samples, failing QC or with nonendometrioid histology on central pathology review, 695 cases were informative for analysis (329 from PORTEC-1, and 366 from PORTEC-2), of which 691 (99.6%) were confirmed as stage I. Clinicopathologic characteristics of these were similar to the original trial populations (<10% absolute difference in frequency of any variable), although comparison with excluded cases revealed modest, although statistically significant differences (Supplementary Table S3). Comparison of cases by trial reflected differences in the study inclusion criteria. The median follow-up was 11.2 years (12.4 years in PORTEC-1 and 10.5 in PORTEC-2).

Immune cell density by clinicopathologic factors and molecular endometrial cancer subgroups

Increased density of tumor-infiltrating $CD8^+$ cytotoxic T cells predicts favorable prognosis in multiple tumor types (36), and previous work has suggested that in endometrial cancer, it is the intraepithelial subset defined by coexpression of CD103, which confer prognostic value (37). We therefore combined an image classification approach using deep neural networks with digital pathology methods quantifying both the density of single positive ($CD8^+$ $CD103^-$ and $CD8^-$ $CD103^+$) and double positive ($CD8^+$ $CD103^+$) cells, and their localization within the intraepithelial or intrastromal compartment (**Fig. 1A**; Supplementary Table S4). Analysis of the 695 cases revealed

Table 1. Characteristics of study participants.

Characteristics	PORTEC-1 *n* = 329	PORTEC-2 *n* = 366	Total *n* = 695	*P*
Age: median (IQR)	67 (13)	66 (12)	70 (10)	<0.0001
Stage (2009 classification)				
IA	126 (38.3%)	59 (16.1%)	185 (26.6%)	<0.0001
IB	203 (61.7%)	303 (82.8%)	506 (72.8%)	
>IB[a]	0 (0.0%)	4 (1.0%)	4 (0.6%)	
Grade				
1	225 (68.4%)	292 (79.8%)	517 (74.4%)	0.014[b]
2	51 (15.5%)	39 (10.7%)	90 (12.9%)	
3	53 (16.1%)	35 (9.6%)	88 (12.7%)	
Myometrial invasion				
≤50%	126 (38.3%)	58 (15.8%)	184 (26.5%)	<0.0001
>50%	203 (61.7%)	308 (84.2%)	511 (73.5%)	
LVSI (none–mild vs. severe)				
None	278 (84.5%)	282 (77.0%)	560 (80.6%)	0.86[c]
Mild	22 (6.7%)	47 (12.8%)	69 (9.9%)	
Severe	14 (4.3%)	17 (4.6%)	31 (4.5%)	
Unknown	15 (4.6%)	20 (5.5%)	35 (5.0%)	
L1CAM				
None or ≤10% positive cells	313 (95.1%)	342 (93.4%)	655 (94.2%)	0.41
>10% positive cells	16 (4.9%)	23 (6.3%)	39 (5.6%)	
Unknown	0 (0.0%)	1 (0.3%)	1 (0.1%)	
Molecular group				
NSMP	177 (55.3%)	212 (59.7%)	389 (57.6%)	0.79
POLE	20 (6.3%)	17 (4.8%)	37 (5.5%)	
MMRd	98 (30.6%)	102 (28.7%)	200 (29.6%)	
p53-mutant	25 (7.8%)	24 (6.8%)	49 (7.3%)	
Unknown	9 (2.7%)	11 (3.0%)	20 (2.9%)	
Received adjuvant treatment[d]				
None	172 (52.3%)	3 (0.8%)	175 (25.5%)	<0.0001
Vaginal brachytherapy	0 (0.0%)	184 (50.3%)	336 (48.3%)	
Pelvic EBRT	157 (47.7%)	179 (48.9%)	184 (26.5%)	

Note: Comparison of cases included in this biomarker study with those excluded and the total trial populations are provided in Supplementary Table S2.
Abbreviations: EBRT, external beam radiotherapy; IQR, interquartile range; L1CAM, L1 cell adhesion molecule; LVSI, lymphovascular space invasion; MMRd, DNA mismatch repair deficient; NSMP, no specific molecular profile; p53-mutant, mutant p53 staining pattern on IHC or *TP53* mutation; *POLE*, pathogenic POLE exonuclease domain mutant.
[a]Includes four cases for which staging was revised following central pathologic review: two cases as stage II and two cases as stage IIIA.
[b]Comparison of proportion of grade 3 versus grade 1–2.
[c]Comparison of severe LVSI versus none or mild.
[d]Adjuvant chemotherapy given in either study.

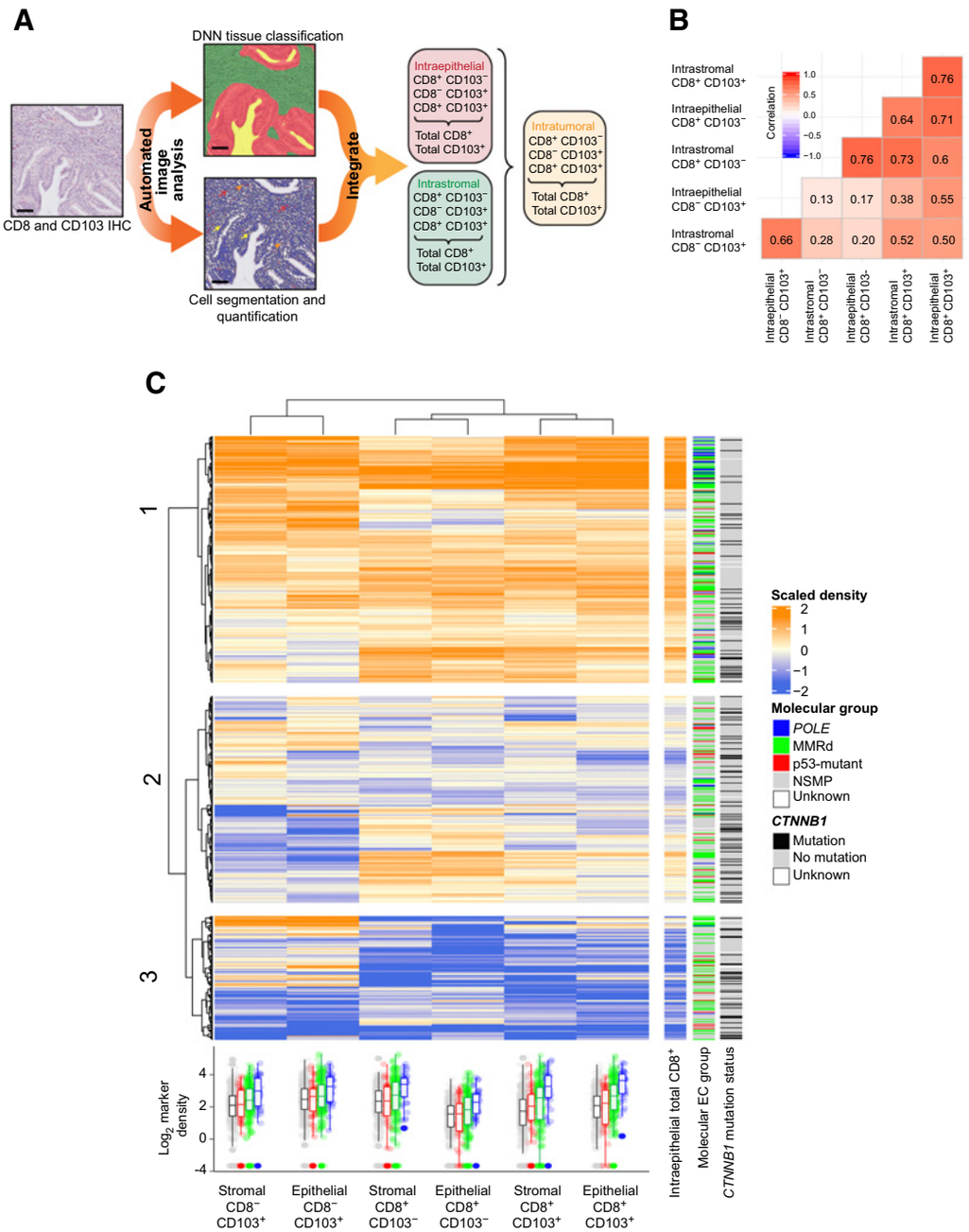

Figure 1.

CD8$^+$ and CD103$^+$ cell density by location and relationship with molecular factors. **A,** Following dual-marker IHC, an image-based, machine-learning algorithm was developed to quantify the density of immune cells expressing the cytotoxic T-cell marker CD8 and/or the intraepithelial T-cell marker CD103 within the intraepithelial and intrastromal compartments. In addition to CD8$^+$ CD103$^-$ cells (red arrows), CD8$^-$ CD103$^+$ cells (yellow arrows), and CD8$^+$ CD103$^+$ cells (orange arrowheads), we analyzed the total number of CD8$^+$ cells (irrespective of CD103 status) and total number of CD103$^+$ cells (irrespective of CD8 status) in these regions separately and in combination (intratumoral density) to give a total of 15 marker–compartment combinations. **B,** Matrix showing Spearman correlation between cell populations by cell surface markers and localization. Densities of total CD8$^+$ and total CD103$^+$ cells in all compartments, and all intratumoral marker densities were excluded, as these are determined by the densities of subpopulations and within subregions. **C,** Unsupervised hierarchical clustering of immune cell densities following mean centering and scaling, using identical marker–compartment combinations as **B**. Cluster number (i.e., dendrogram cut height) was selected based on the results of the gap statistic. Bars to the right of the heatmap show density of intratumoral and intraepithelial CD8$^+$ cell density, TCGA molecular subgroup, and CTNNB1 mutation status. Boxplots below heatmap indicate cell density by TCGA subgroup for each marker–compartment combination (shown in full in Supplementary Fig. S3). Lower and upper limits of box indicate 25th and 75th percentiles; whiskers extend to 1.5× interquartile range below and above these values, respectively; and horizontal line within box indicates median. DNN, deep neural network; EC, endometrial cancer; MMRd, DNA mismatch repair deficient; NSMP, no specific molecular profile; *POLE*, pathogenic POLE exonuclease domain mutant; p53-mutant, mutant p53 staining pattern on IHC or *TP53* mutation.

substantial variation in both the density of these cells and in that of total $CD8^+$ cells and total $CD103^+$ cells across tumors, with marked positive skewness (3.56–5.88; Supplementary Table S5; Supplementary Fig. S2). As anticipated, the density of immune infiltrate was positively correlated between markers and compartments, although the strength of this relationship was variable (Spearman $\rho = 0.13$–0.76), with the most significant correlation for $CD8^+$ single-positive and $CD8^+$ $CD103^+$ double-positive cells between the intraepithelial and intrastromal compartments (**Fig. 1B**). Although the density of total $CD8^+$ cells was lower in the intraepithelial than intrastromal compartment (mean 31.1 vs. 41.9 cells/mm^2, $P = 1.8 \times 10^{-5}$, Mann–Whitney test), the opposite was true of $CD8^+$ $CD103^+$ double positive cells (mean 20.4 vs. 12.1 cells/mm^2, $P = 1.8 \times 10^{-5}$), consistent with the known role of CD103 in intraepithelial localization (37).

Unsupervised hierarchical clustering of cases by immune marker density and compartment suggested three groups with high, intermediate and low immune cell infiltrate, with highly significant variation in the proportion of molecular endometrial cancer subtypes between them ($P = 8.3 \times 10^{-6}$; **Fig. 1C**; Supplementary Fig. S3). The immune-high group contained more than three quarters of *POLE*-mutant cases (29/37; 78.4%), and a majority of the MMRd tumors (103/200; 51.5%), but proportionally fewer NSMP tumors (140/389; 36.0%). This group also contained the largest proportion of p53-mutant tumors (20/49; 40.8%); an unexpected finding given the poor prognosis of this group. In contrast, the immune-low group contained only 2 (5.4%) *POLE*-mutant tumors, but approximately one fifth of MMRd (40/200; 20%) and NSMP (90/389; 23.1%) cases. Interestingly, given recent data linking Wnt pathway activation with immune exclusion in tumors (38), mutation of *CTNNB1*, which encodes a key Wnt mediator was significantly enriched in the low (32/140; 22.9%) and intermediate (51/246; 20.7%) immune subgroups, compared with the high subgroup (41/284; 14.4%, $P = 0.019$). Multiple linear regression revealed that *POLE* mutation and, to a lesser extent, MMRd were strongly predictive of immune infiltrate across all marker–compartment combinations examined, while age, myometrial invasion, grade, and *CTNNB1* mutation were less reliably associated, and LVSI, L1CAM overexpression, and p53 mutation showed no obvious association (Supplementary Table S6).

Prognostic value of immune cell infiltrate

We proceeded to examine the potential association of immune cell density with disease recurrence, mindful that this may vary by both cell type and compartment. We extended our previous analysis of $CD8^+$ and $CD103^+$ single positive cells and double positive cells to include total $CD8^+$ cells (i.e., irrespective of CD103 status) and total $CD103^+$ cells (i.e., irrespective of CD8 status) and to include analysis of the entire tumor region including both epithelial and stromal compartments. Univariable analysis of all 15 marker–compartment combinations in the pooled trial population with internal bootstrap validation ($n = 1{,}000$) revealed that $CD8^+$ $CD103^-$ single positive cells in either the epithelial compartment or combined epithelial and stromal compartments, and intraepithelial total $CD8^+$ density were the strongest predictors of tumor recurrence (Supplementary Table S7). Of these, intraepithelial $CD8^+$ density was selected for further analysis on the basis of its effect size [HR = 0.88 per 2-fold increase; 95% confidence interval (CI), 0.82–0.95; $P = 0.001$], Akaike information criterion, and clinical applicability of a single immunostain. Interestingly, and in contrast to other malignancies (39), intrastromal immune infiltrate had no discernible prognostic value.

Integration of molecular endometrial cancer classification and image-based immunoprofiling

We next examined whether quantification of intraepithelial total $CD8^+$ cell density could further enhance risk stratification beyond the improvement the molecular endometrial cancer classification (including L1CAM positivity) provides over clinicopathologic variables alone (11). We first confirmed that addition of these molecular factors improved prediction of disease recurrence and goodness of model fit compared with a "pathologic" multivariable model containing clinicopathologic variables only (LR test $P = 1.2 \times 10^{-6}$; Supplementary Table S8). Addition of intraepithelial $CD8^+$ cell density to this "molecular" model further improved model fit (LR test $P = 3.0 \times 10^{-3}$), and confirmed the independent prognostic value of this marker, with multivariable-adjusted HR of 0.88 for each 2-fold increase (95% CI, 0.81–0.95; $P = 1.8 \times 10^{-3}$; **Table 2**; **Fig. 2A**). This association was essentially unchanged after exclusion of the four (0.6%) cases reclassified as stage II/IIIA by central review, by the inclusion of *CTNNB1* mutation in the multivariable model, or by exclusion of grade 3 and *POLE*-mutant cases (Supplementary Tables S9–S11). The prognostic value of intraepithelial $CD8^+$ density equated to a multivariable-adjusted HR of 0.70 (95% CI, 0.57–0.88) for comparison of cases with a density at the 75th percentile versus those at the 25th percentile, and a HR of 0.50 (95% CI, 0.33–0.78) for cases at the 90th percentile versus those at the 10th percentile (**Fig. 2A**). Corresponding point estimates of the likelihood of being recurrence-free at 3 years were 88.1% (95% CI, 84.0%–92.3%), 89.9% (86.7%–93.3%), 92.6% (89.7%–95.6%), and 93.5% (90.6%–96.5%), for cases at the 10th, 25th, 75th, and 90th percentile of $CD8^+$ cell density respectively. The prognostic value of intraepithelial $CD8^+$ cell density was also observed when dichotomized at the sample median (multivariable-adjusted HR for high vs. low = 0.50; 95% CI, 0.31–0.81; $P = 5.1 \times 10^{-3}$; **Fig. 2B**). Sensitivity analysis showed no evidence that these results were due to differential effect of radiotherapy by $CD8^+$ cell density (Supplementary Table S12).

Comparison of multivariable models with internal bootstrap validation demonstrated that the molecular-immune model had the highest concordance, confirming the independent prognostic value of both the molecular endometrial cancer classification and immune infiltrate (**Table 2**; **Fig. 2C**). Further analysis of this molecular-immune model revealed that intraepithelial $CD8^+$ cell density was a more important predictor of recurrence than myometrial invasion, tumor grade, or L1CAM positivity (**Fig. 2D**). Intraepithelial $CD8^+$ cell infiltrate was also predictive of endometrial cancer–specific survival in multivariable analysis both as a continuous variable (HR = 0.89; 95% CI, 0.81–0.98; $P = 0.015$) and when dichotomized (HR = 0.47; 95% CI, 0.26–0.87; $P = 0.016$; **Table 2**; Supplementary Fig. S3).

Prognostic value of intraepithelial $CD8^+$ infiltrate within TCGA subgroups and by *CTNNB1* mutation

The unexpectedly high prevalence of p53-mutant cases in the immune high cluster, and the lack of association of MMRd with reduced recurrence despite typically prominent T-cell infiltrate motivated us to explore the prognostic value of intraepithelial $CD8^+$ infiltrate within endometrial cancer molecular subgroups. $CD8^+$ cell density was a statistically significant predictor of recurrence in the p53-mutant subgroup ($n = 47$) in univariable analysis (HR = 0.84; 95% CI, 0.73–0.97; $P = 0.017$), and after adjusting for grade and LVSI in multivariable analysis (HR = 0.84; 95% CI, 0.73–0.98; $P = 0.024$; **Table 3**; **Fig. 3A**). A similar, albeit weaker association was evident in the NSMP subgroup ($n = 374$), although this fell just outside the margin of statistical significance in multivariable analysis (univariable HR = 0.88; 95% CI, 0.77–1.00; $P = 0.048$, adjusted HR =

Table 2. Univariable and multivariable analyses of time to endometrial cancer recurrence and endometrial cancer–specific survival in pooled PORTEC-1 and PORTEC-2 trial population.

	Univariable analysis		Multivariable analysis	
	HR (95% CI)	***P***	**HR (95% CI)**	***P***
Endometrial cancer recurrence (640 cases, 80 events)				
Myometrial invasion				
≤50%	1.0 (ref)	—	1.0 (ref)	—
>50%	1.46 (0.88–2.43)	0.15	2.39 (1.32–4.30)	3.9×10^{-3}
Grade				
1–2	1.0 (ref)	—	1.0 (ref)	—
3	2.49 (1.53–4.03)	0.00022	2.21 (1.25–3.91)	6.4×10^{-3}
LVSI				
Absent/mild	1.0 (ref)	—	1.0 (ref)	—
Severe	3.25 (1.67–6.30)	0.00051	4.19 (2.09–8.38)	5.1×10^{-5}
L1CAM				
≤10% staining	1.0 (ref)	—	1.0 (ref)	—
>10% staining	4.70 (2.69–8.21)	5.5×10^{-8}	2.26 (1.12–4.53)	0.022
Molecular group of endometrial cancer				
NSMP	1.0 (ref)	—	1.0 (ref)	—
POLE	0.80 (0.25–2.58)	0.71	1.41 (0.41–4.75)	0.59
MMRd	1.43 (0.88–2.33)	0.15	1.30 (0.75–2.23)	0.35
p53-mutant	4.84 (2.76–8.48)	3.5×10^{-8}	4.98 (2.51–9.88)	4.2×10^{-6}
Intraepithelial $CD8^+$ cell density (continuous, per doubling)	0.89 (0.82–0.96)	0.0036	0.88 (0.81–0.95)	1.9×10^{-3}
Endometrial cancer–specific survival (640 cases, 53 events)				
Myometrial invasion				
≤50%	1.0 (ref)	—	1.0 (ref)	—
>50%	1.20 (0.66–2.19)	0.55	2.22 (1.10–4.48)	0.026
Grade				
1–2	1.0 (ref)	—	1.0 (ref)	—
3	3.50 (2.03–6.04)	6.6×10^{-6}	2.58 (0.33–4.99)	5.1×10^{-3}
LVSI				
Absent/mild	1.0 (ref)	—	1.0 (ref)	—
Severe	3.94 (1.86–8.37)	0.00035	5.33 (2.37–11.98)	5.2×10^{-5}
L1CAM				
≤10% staining	1.0 (ref)	—	1.0 (ref)	—
>10% staining	5.19 (2.75–9.79)	3.6×10^{-7}	2.26 (1.03–4.96)	0.043
Molecular group of endometrial cancer				
NSMP	1.0 (ref)	—	1.0 (ref)	—
POLE	1.01 (0.24–4.32)	0.99	1.70 (0.38–7.62)	0.49
MMRd	2.12 (1.16–3.86)	0.014	1.68 (0.84–3.34)	0.14
p53-mutant	7.35 (3.78–14.3)	4.0×10^{-9}	6.79 (3.3–15.22)	3.2×10^{-6}
Intraepithelial $CD8^+$ cell density (continuous, per doubling)	0.88 (0.80–0.97)	0.0077	0.89 (0.81–0.98)	0.015

Note: Cox models use all informative cases and exclude those with missing data in case of multivariable models (maximum 5.0% missing data for any variable). Multivariable models included prespecified covariables of known prognostic value (see Materials and Methods) and were not subject to variable selection. Results from corresponding Cox models for endometrial cancer recurrence and endometrial cancer–specific survival before and after addition of $CD8^+$ cell density are provided in Supplementary Table S5. Results from analysis after exclusion of the four (0.6%) cases classified as > stage I on central review are shown in Supplementary Table S6. The addition of intraepithelial $CD8^+$ cell density to the molecular model (containing clinicopathologic variables, the molecular endometrial cancer classifier, and L1CAM) for endometrial cancer recurrence was associated with an improvement in model fit evidenced by: (i) reduction in Akaike information criterion (AIC; molecular model vs. integrated molecular-immune model = 842.2 vs. 835.4), (ii) increase in model concordance (C index 0.697 vs. 0.726), and (iii) likelihood ratio test for comparison of nested models: $P = 3.0 \times 10^{-3}$). Similar, albeit less strong, results were obtained from comparison of models for endometrial cancer–specific survival (molecular model vs. molecular-immune model): (i) AIC = 544.9 versus 541.4, (ii) C index 0.792 versus 0.802, and (iii) likelihood ratio test for comparison of models: $P = 0.019$.

Abbreviations: CI, confidence interval; HR, hazard ratio; L1CAM, L1 cell adhesion molecule; LVSI, lymphovascular space invasion; MMRd, DNA mismatch repair deficient; NSMP, no specific molecular profile; p53-mutant, mutant p53 staining pattern on IHC or *TP53* mutation; *POLE*, pathogenic POLE exonuclease domain mutant.

0.88; 95% CI, 0.77–1.00; $P = 0.055$, respectively; **Table 3**; **Fig. 3A**). In contrast, among MMRd tumors ($n = 186$), $CD8^+$ infiltrate had no detectable prognostic value (univariable HR = 0.98; 95% CI, 0.84–1.16; $P = 0.85$, adjusted HR = 0.95; 95% CI, 0.79–1.13; $P = 0.56$; **Fig. 3B**). The small number of cases and events in the POLE-mutant subgroup precluded similar analysis (**Table 3**; **Fig. 3B**). Further exploratory analysis by *CTNNB1* mutation revealed $CD8^+$ density held similar prognostic value among wild-type cases as the total study population (HR = 0.86; 95% CI, 0.79–0.94; $P = 1.1 \times 10^{-3}$); the modest size of the *CTNNB1*-mutant subgroup precluded firm conclusions (Supplementary Table S13).

Concordance between AI-based quantification and pathologist-based estimation of tumor $CD8^+$ cell infiltration

Although CD8 IHC is a standard assay in pathology laboratories, AI-based image analysis and quantification is, at present, limited to the

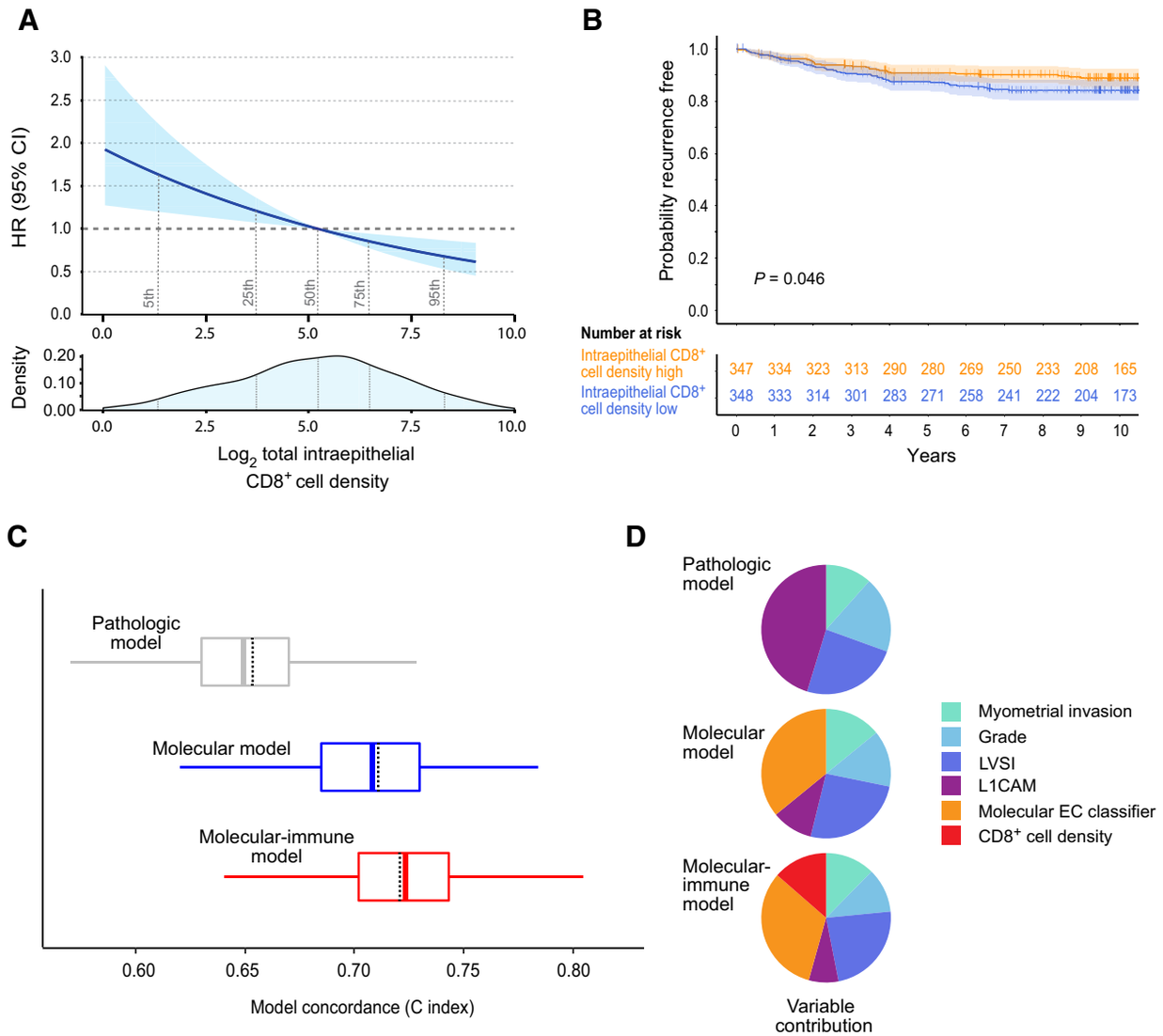

Figure 2.

Prognostic value of intraepithelial total CD8$^+$ infiltrate in pooled study population. **A,** Top, plot showing HR for endometrial cancer recurrence according to ($\log_2$-transformed) density of intraepithelial total CD8$^+$ cells after adjusting for covariables. Note that each unit increase corresponds to a doubling in marker density. Bottom, corresponding kernel density plot showing proportion of cases according to density of immune infiltrate. Dashed vertical lines correspond to 5th, 25th, 50th, 75th, and 95th percentiles. **B,** Kaplan–Meier curves showing time to endometrial cancer recurrence by intraepithelial total CD8$^+$ density divided at the sample median. *P* value was determined by the log-rank test; shaded area indicates 95% CI. **C,** Boxplots showing concordance (C index) of base model (pathologic factors only), molecular model (pathologic factors plus molecular endometrial cancer classifier and L1CAM expression), and integrated molecular-immune model (molecular model plus intraepithelial total CD8$^+$ density for time to endometrial cancer recurrence). Box and whisker (Tukey) plots use results of 1,000 bootstrap resamples from study population; lower and upper limits of box indicate 25th and 75th percentiles; and whiskers extend to 1.5× interquartile range below and above these values, respectively. Thick, vertical colored lines within box indicate median value from bootstrap resamples; dashed vertical line indicates C index from original biomarker population. **D,** Pie charts showing relative importance of variables within these three multivariable models based on the proportion of the χ^2 statistic. CI, confidence interval; HR, hazard ratio; L1CAM, L1 cell adhesion molecule; LVSI, lymphovascular space invasion.

research setting. We therefore sought to determine whether a simple pathologist estimation of intraepithelial CD8$^+$ cell infiltrate could serve as a surrogate for AI-based quantification for future study. Taking CD8$^+$ cell counts (i.e., the number of intraepithelial cells within each TMA core) as a measure readily amenable to pathologist estimation (in contrast to density, which requires determination of the area under analysis), we defined four groups, broadly corresponding to the quartiles determined by AI-based analysis (0–5, 5–15, 15–50, and >50 cells per TMA core). A subset of 100 cases were then independently reviewed by three pathologists, and assigned to these groups, each blinded to the results of the others and the AI-based analysis. Analysis of the results revealed substantial to strong concordance between individual pathologist categorization (weighted Cohen kappa 0.70–0.89, all $P < 0.001$), and moderate to substantial concordance between individual and consensus pathologic categorization and the AI-based algorithm (kappa 0.4–0.65; Supplementary Table S14). On

Table 3. Exploratory univariable and multivariable analyses of time to endometrial cancer recurrence according to molecular endometrial cancer subgroup.

	Univariable analysis		Multivariable analysis	
	HR (95% CI)	***P***	**HR (95% CI)**	***P***
NSMP (374 cases, 35 events)				
Grade				
1–2	1.0 (ref)	—	1.0 (ref)	—
3	4.55 (1.95–10.65)	4.7×10^{-4}	5.61 (2.23–14.13)	2.5×10^{-4}
LVSI				
Absent/mild	1.0 (ref)	—	1.0 (ref)	—
Severe	3.14 (0.95–10.45)	0.062	3.09 (0.92–10.41)	0.068
$CD8^+$ cell density (continuous)	0.88 (0.77–0.999)	0.048	0.88 (0.77–1.00)	0.055
POLE (34 cases, 3 events)	Not done	—	Not done	—
MMRd (186 cases, 24 events)				
Grade				
1–2	1.0 (ref)	—	1.0 (ref)	—
3	1.43 (0.60–3.37)	0.41	1.16 (0.45–3.01)	0.75
LVSI				
Absent/mild	1.0 (ref)	—	1.0 (ref)	—
Severe	4.97 (2.03–12.13)	4.4×10^{-4}	4.91 (1.96–12.3)	6.8×10^{-4}
$CD8^+$ cell density (continuous)	0.98 (0.84–1.16)	0.85	0.95 (0.79–1.13)	0.56
p53-mutant (47 cases, 18 events)				
Grade				
1–2	1.0 (ref)	—	1.0 (ref)	—
3	1.39 (0.54–3.56)	0.49	1.12 (0.41–3.04)	0.82
LVSI[a]	—	—	—	—
$CD8^+$ cell density (continuous)	0.84 (0.73–0.97)	0.017	0.84 (0.73–0.98)	0.024

Note: Univariable and multivariable HRs are derived from complete case analyses and exclude cases with missing data (maximum 7.0% for any single variable). Analysis of POLE subgroup was not performed due to the very small number of events within this subset. Covariables of tumor grade and LVSI used in multivariable analyses were prespecified based upon prognostic value in pooled study population; variable selection was not performed.

Abbreviations: CI, confidence interval; HR, hazard ratio; L1CAM, L1 cell adhesion molecule; LVSI, lymphovascular space invasion; MMRd, DNA mismatch repair deficient; NSMP, no specific molecular profile; p53-mutant, mutant p53 staining pattern on IHC or *TP53* mutation; *POLE*, pathogenic POLE exonuclease domain mutant.

[a]Failure of model convergence precluded analysis of LVSI within the p53-mutant subgroup.

review, this difference was determined to be due to systematic underscoring by the pathologists compared with the AI-based method, that is, the AI-based method demonstrated greater sensitivity. Although pathologist evaluation of the entire study population was beyond the scope of this study, these could serve as pragmatic cutoff points for future validation.

Discussion

In this study, we show that machine-learning, image-based quantification of intraepithelial $CD8^+$ cells refines prognostication in early-stage endometrioid endometrial cancer beyond clinicopathologic and molecular factors. Our multimodal approach holds promise to improve risk stratification, and thus reduce over- and undertreatment in this common cancer.

Although previous studies have shown the strong prognostic value of the molecular endometrial cancer classification (11, 16), and of the density of tumor-infiltrating lymphocytes in endometrial cancer (19, 20), to our knowledge our study is one of only two to examine the combination of these factors. The other study, by Talhouk and colleagues (23), reported no prognostic effect of intraepithelial $CD3^+$ $CD8^+$ cells in multivariable analysis, which included the molecular endometrial cancer classification, although a tendency to improved survival was observed. The discordance with our results is currently unexplained, but may relate to the methodology used for immune cell localization, statistical analysis, or the smaller, nontrial population of mixed histotypes and stages used in their study.

Interestingly, and also in contrast to Talhouk and colleagues' results (23), our data suggest that image-based assessment of immune infiltrate has particular value in specific molecular subgroups. The first are low mutation burden NSMP tumors, which constitute the majority of early-stage endometrioid endometrial cancer and which currently lack reliable molecular stratifiers. The second are low mutation burden p53-mutant cases, which have poor prognosis and are increasing in prevalence (40). In contrast, we found no evidence that intraepithelial $CD8^+$ cell density was prognostic in high mutation burden MMRd tumors, despite their overall enhanced T-cell infiltrate compared with NSMP and p53-mutant subgroups. The reasons for this discrepancy are unclear. Although it is tempting to speculate on the antigenicity of SCNAs in p53-mutant tumors, or attenuation of T cell–mediated cytotoxicity by immune checkpoint upregulation in MMRd cases, these exploratory analyses require validation before conclusions can be drawn and mechanisms investigated.

Strengths of our study include its large size, homogeneous clinical trial cohorts with meticulous follow-up data (3, 4), central pathologic review, and comprehensive annotation of pathologic and molecular

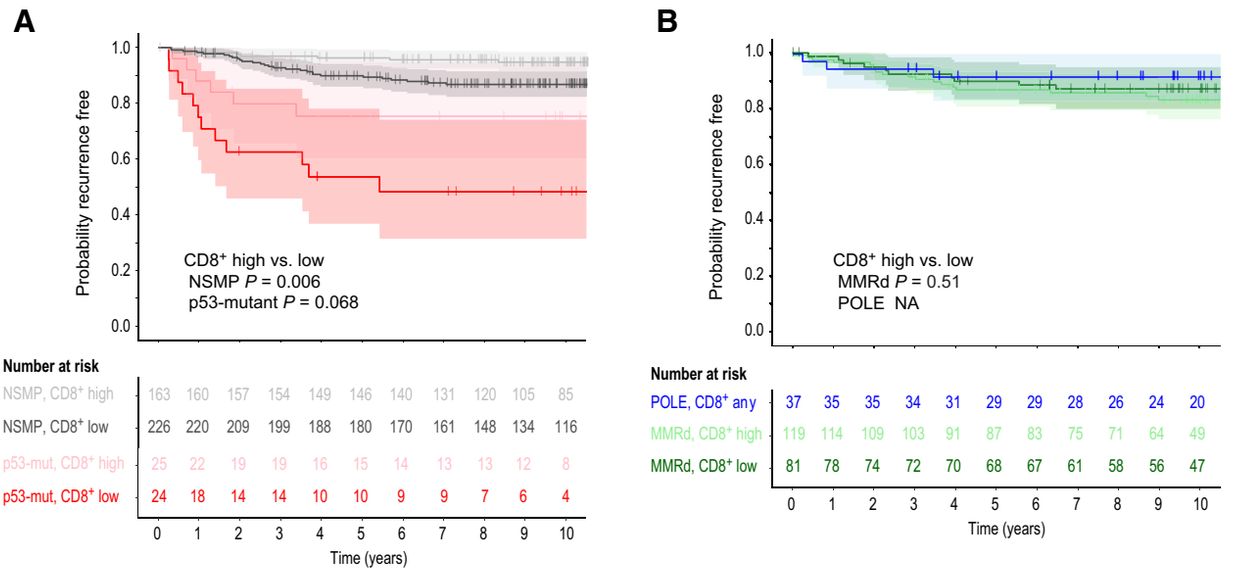

Figure 3.

Prognostic value of intraepithelial CD8$^+$ cell infiltrate within molecular endometrial cancer subgroups. Kaplan–Meier curves showing probability of endometrial cancer recurrence according to intraepithelial total CD8$^+$ cell density (dichotomized at median of study population) for NSMP and p53-mutant tumors (**A**), characterized by low mutation burden, and MMRd and POLE tumors (**B**), characterized by high mutation burden (POLE subgroup was not subdivided, as only three cases had CD8$^+$ cell densities below the study median). *P* values were calculated by the log-rank test; shaded area indicates 95% CI. CD8$^+$, intraepithelial total CD8$^+$ cell density; MMRd, DNA mismatch repair deficient; NSMP, no specific molecular profile; *POLE*, pathogenic POLE exonuclease domain mutant; p53-mutant, mutant p53 staining pattern on IHC or *TP53* mutation.

risk factors (11). Another strength is our combination of machine learning–based image segmentation methods with digital pathology to enable automated analysis of the type, density, and localization of T cells, the importance of which is illustrated by the differing prognostic value of intraepithelial and intrastromal infiltrates. Our approach is readily implementable with a single immunostain in routine clinical use, and thus represents an advance on previous methods, which rely on manual cell counting or multispectral analysis, neither of which are deliverable at the scale required for clinical practice.

Our study has limitations. For logistic reasons, we used TMAs rather than whole tissue sections. Given the potential for intratumoral heterogeneity in both molecular alterations (e.g., subclonal MMR loss) and immune infiltrate in tumors, it will be important to determine whether our results could be improved by analysis of a larger tissue area, ideally including the tumor invasive margin. Similar considerations limited our focus mainly to cytotoxic T cells; it will also be of interest to see whether analysis of additional immune cell types improves prognostication, notwithstanding the issues of scalability noted above. Finally, although chemotherapy was not used in our study population, it is theoretically possible that our results could reflect enhanced radiosensitivity in CD8$^+$ high tumors, although sensitivity analysis did not support this.

Although our results illustrate the potential of digital pathology to improve clinical care, the infrastructure required to implement this is currently limited to specialist centers. We therefore evaluated whether a simple categorization of cases by pathologists according to CD8$^+$ cell infiltrate could serve as a surrogate for the AI-based quantification. The good concordance between methods suggests that, with validation, the cutoff points we define could be used in clinical practice in the near-term. However, the pragmatic, semiquantitative pathologist-based assessment was generally less sensitive than the AI-based classifier. This highlights that cutoffs for immune cell assessment are method-dependent and underscores the advantage of deriving continuous scores using unbiased, automated methods for image analysis at single-cell resolution.

To conclude, we show that image-based quantification of intraepithelial CD8$^+$ cells improves the strength of the molecular endometrial cancer classification and refines prognostication in early-stage endometrioid endometrial cancer. Future work will seek to validate this finding, particularly in higher risk cohorts including nonendometrioid histotypes such as the PORTEC-3 study (6), and to validate this novel multimodal approach for clinical implementation.

Disclosure of Potential Conflicts of Interest

M. de Bruyn reports grants from Dutch Cancer Society, European Research Council, Health Holland, and DCPrime, grants and nonfinancial support from Aduro Biotech, and nonfinancial support from AIMM Therapeutics, BioNTech, Surflay, and Vicinivax outside the submitted work, as well as a patent for antibodies targeting CD103 (de Bruyn et al., no. 62/704,258) pending. E. Stelloo reports grants from Dutch Cancer Society (UL2012-5719) during the conduct of the study. C.L. Creutzberg reports grants from Dutch Cancer Society (PORTEC-1 and -2 clinical trial grants) during the conduct of the study, as well as grants from Dutch Cancer Society (PORTEC-4a research grant) outside the submitted work. H.W. Nijman reports grants and nonfinancial support from Dutch Cancer Society and Aduro Biotech, grants from Health Holland, DCPrime, and The Dutch Research Council, nonfinancial support from AIMM Therapeutics and BioNTech, and grants, nonfinancial support, and other from Vicinivax (shareholder) outside the submitted work, as well as a patent for antibodies targeting CD103 (de Bruyn et al., no. 62/704,258) pending. V.H. Koelzer reports grants from Promedica Foundation (F-87701-41-01) during the conduct of the study, other from Indica Labs (invited speaker on behalf of Indica Labs) outside the submitted work, as well as a patent for nl 73455NL pending [participant of a patent application co-owned by the Netherlands Cancer Institute (NKI-AVL) and the University of Basel on the assessment of cancer immunotherapy biomarkers by digital pathology]. No potential conflicts of interest were disclosed by the other authors.

Disclaimer

The views expressed are those of the authors and not necessarily those of the NHS, the NIHR, the Department of Health, or the Wellcome Trust.

Authors' Contributions

N. Horeweg: Conceptualization, data curation, formal analysis, visualization, methodology, writing–original draft, writing–review and editing. **M. de Bruyn:** Conceptualization, formal analysis, methodology, writing–review and editing. **R.A. Nout:** Resources, formal analysis, writing–review and editing. **E. Stelloo:** Resources, writing–review and editing. **K. Kedzierska:** Formal analysis, visualization, methodology, writing–review and editing. **A. León-Castillo:** Formal analysis, writing–review and editing. **A. Plat:** Resources, writing–review and editing. **K.D. Mertz:** Resources, writing–review and editing. **M. Osse:** Resources, writing–review and editing. **I.M. Jürgenliemk-Schulz:** Resources, writing–review and editing. **L.C.H.W. Lutgens:** Resources, writing–review and editing. **J.J. Jobsen:** Resources, writing–review and editing. **E.M. van der Steen-Banasik:** Resources, writing–review and editing. **V.T. Smit:** Resources, writing–review and editing. **C.L. Creutzberg:** Resources, data curation, writing–review and editing. **T. Bosse:** Conceptualization, resources, formal analysis, methodology, writing–review and editing. **H.W. Nijman:** Resources, supervision, writing–review and editing. **V.H. Koelzer:** Conceptualization, formal analysis, investigation, methodology, writing–review and editing. **D.N. Church:** Conceptualization, formal analysis, supervision, investigation, visualization, methodology, writing–original draft, writing–review and editing.

Acknowledgments

The PORTEC-1 and PORTEC-2 trials were supported by grants from the Dutch Cancer Society (CKTO 90–01 and CKTO 2001–04, respectively). This study was supported by a translational research project grant from the Dutch Cancer Society (UL2012–5719), the Oxford NIHR Comprehensive Biomedical Research Centre (BRC), and core funding to the Wellcome Trust Centre for Human Genetics from the Wellcome Trust (090532/Z/09/Z). K. Kedzierska is supported by a Genomic Medicine and Statistics Studentship from the Wellcome Trust. T. Bosse is supported by a Dutch Cancer Society Young Investigator Award. V.H. Koelzer is supported by the Promedica Foundation (F-87701–41–01). D.N. Church is funded by a Cancer Research UK Advanced Clinician Scientist Fellowship and was previously supported by a Health Foundation/Academy of Medical Sciences Clinician Scientist Fellowship (grant reference C26642/A27963). The authors are grateful to the participants in the PORTEC-1 and PORTEC-2 trial, and to the investigators and pathologists who recruited patients and collected samples.

The costs of publication of this article were defrayed in part by the payment of page charges. This article must therefore be hereby marked *advertisement* in accordance with 18 U.S.C. Section 1734 solely to indicate this fact.

Received February 18, 2020; revised July 2, 2020; accepted September 24, 2020; published first September 30, 2020.

References

1. Ferlay J, Steliarova-Foucher E, Lortet-Tieulent J, Rosso S, Coebergh JW, Comber H, et al. Cancer incidence and mortality patterns in Europe: estimates for 40 countries in 2012. Eur J Cancer 2013;49:1374–403.
2. Siegel RL, Miller KD, Jemal A. Cancer statistics, 2019. CA Cancer J Clin 2019;69;7–34.
3. Creutzberg CL, van Putten WL, Koper PC, Lybeert ML, Jobsen JJ, Warlam-Rodenhuis CC, et al. Surgery and postoperative radiotherapy versus surgery alone for patients with stage-1 endometrial carcinoma: multicentre randomised trial. PORTEC Study Group. Post operative radiation therapy in endometrial carcinoma. Lancet 2000;355;1404–11.
4. Nout RA, Smit VT, Putter H, Jurgenliemk-Schulz IM, Jobsen JJ, Lutgens LC, et al. Vaginal brachytherapy versus pelvic external beam radiotherapy for patients with endometrial cancer of high-intermediate risk (PORTEC-2): an open-label, non-inferiority, randomised trial. Lancet 2010;375:816–23.
5. Wortman BG, Creutzberg CL, Putter H, Jurgenliemk-Schulz IM, Jobsen JJ, Lutgens L, et al. Ten-year results of the PORTEC-2 trial for high-intermediate risk endometrial carcinoma: improving patient selection for adjuvant therapy. Br J Cancer 2018;119:1067–74.
6. de Boer SM, Powell ME, Mileshkin L, Katsaros D, Bessette P, Haie-Meder C, et al. Adjuvant chemoradiotherapy versus radiotherapy alone for women with high-risk endometrial cancer (PORTEC-3): final results of an international, open-label, multicentre, randomised, phase 3 trial. Lancet Oncol 2018;19:295–309.
7. Creutzberg CL, Lu KH, Fleming GF. Uterine cancer: adjuvant therapy and management of metastatic disease. J Clin Oncol 2019;37:2490–500.
8. Colombo N, Creutzberg C, Amant F, Bosse T, Gonzalez-Martin A, Ledermann J, et al. ESMO-ESGO-ESTRO Consensus Conference on Endometrial Cancer: diagnosis, treatment and follow-up. Ann Oncol 2016;27:16–41.
9. Bosse T, Peters EE, Creutzberg CL, Jurgenliemk-Schulz IM, Jobsen JJ, Mens JW, et al. Substantial lympho-vascular space invasion (LVSI) is a significant risk factor for recurrence in endometrial cancer–a pooled analysis of PORTEC 1 and 2 trials. Eur J Cancer 2015;51:1742–50.
10. Kurnit KC, Kim GN, Fellman BM, Urbauer DL, Mills GB, Zhang W, et al. CTNNB1 (beta-catenin) mutation identifies low grade, early stage endometrial cancer patients at increased risk of recurrence. Mod Pathol 2017;30:1032–41.
11. Stello E, Nout RA, Osse EM, Jurgenliemk-Schulz IJ, Jobsen JJ, Lutgens LC, et al. Improved risk assessment by integrating molecular and clinicopathological factors in early-stage endometrial cancer-combined analysis of the PORTEC cohorts. Clin Cancer Res 2016;22:4215–24.
12. Zeimet AG, Reimer D, Huszar M, Winterhoff B, Puistola U, Azim SA, et al. L1CAM in early-stage type I endometrial cancer: results of a large multicenter evaluation. J Natl Cancer Inst 2013;105:1142–50.
13. Liu Y, Patel L, Mills GB, Lu KH, Sood AK, Ding L, et al. Clinical significance of CTNNB1 mutation and Wnt pathway activation in endometrioid endometrial carcinoma. J Natl Cancer Inst 2014;106:dju245.
14. The Cancer Genome Atlas Research Network. Integrated genomic characterization of endometrial carcinoma. Nature 2013;497:67–73.
15. Bosse T, Nout RA, Stelloo E, Dreef E, Nijman HW, Jurgenliemk-Schulz IM, et al. L1 cell adhesion molecule is a strong predictor for distant recurrence and overall survival in early stage endometrial cancer: pooled PORTEC trial results. Eur J Cancer 2014;50:2602–10.
16. Kommoss S, McConechy MK, Kommoss F, Leung S, Bunz A, Magrill J, et al. Final validation of the ProMisE molecular classifier for endometrial carcinoma in a large population-based case series. Ann Oncol 2018;29:1180–8.
17. Costigan DC, Dong F, Nucci MR, Howitt BE. Clinicopathologic and immunohistochemical correlates of CTNNB1 mutated endometrial endometrioid carcinoma. Int J Gynecol Pathol 2020;39:119–27.
18. Wortman BG, Bosse T, Nout RA, Lutgens L, van der Steen-Banasik EM, Westerveld H, et al. Molecular-integrated risk profile to determine adjuvant radiotherapy in endometrial cancer: evaluation of the pilot phase of the PORTEC-4a trial. Gynecol Oncol 2018;151:69–75.
19. Kondratiev S, Sabo E, Yakirevich E, Lavie O, Resnick MB. Intratumoral CD8+ T lymphocytes as a prognostic factor of survival in endometrial carcinoma. Clin Cancer Res 2004;10:4450–56.
20. de Jong RA, Leffers N, Boezen HM, ten Hoor KA, van der Zee AG, Hollema H, et al. Presence of tumor-infiltrating lymphocytes is an independent prognostic factor in type I and II endometrial cancer. Gynecol Oncol 2009;114:105–10.
21. van Gool IC, Eggink FA, Freeman-Mills L, Stelloo E, Marchi E, de Bruyn M, et al. POLE proofreading mutations elicit an antitumor immune response in endometrial cancer. Clin Cancer Res 2015;21:3347–55.
22. Eggink FA, Van Gool IC, Leary A, Pollock PM, Crosbie EJ, Mileshkin L, et al. Immunological profiling of molecularly classified high-risk endometrial cancers identifies POLE-mutant and microsatellite unstable carcinomas as candidates for checkpoint inhibition. Oncoimmunology 2017;6:e1264565.
23. Talhouk A, Derocher H, Schmidt P, Leung S, Milne K, Gilks CB, et al. Molecular subtype not immune response drives outcomes in endometrial carcinoma. Clin Cancer Res 2019;25:2537–48.
24. Nout RA, van de Poll-Franse LV, Lybeert ML, Wárlám-Rodenhuis CC, Jobsen JJ, Mens JWMM, et al. Long-term outcome and quality of life of patients with endometrial carcinoma treated with or without pelvic radiotherapy in the post operative radiation therapy in endometrial carcinoma 1 (PORTEC) trial. J Clin Oncol 2011;29:1692–700.
25. Scholten AN, van Putten WL, Beerman H, Smit VTHBM, Koper PCM, Lybeert MLM, et al. Postoperative radiotherapy for stage 1 endometrial carcinoma: long-term outcome of the randomized PORTEC trial with central pathology review. Int J Radiat Oncol Biol Phys 2005;63:834–8.
26. Church DN, Stelloo E, Nout RA, Valtcheva N, Depreeuw J, ter Haar N, et al. Prognostic significance of POLE proofreading mutations in endometrial cancer. J Natl Cancer Inst 2015;107:402.

27. Stelloo E, Bosse T, Nout RA, MacKay HJ, Church DN, Nijman HW, et al. Refining prognosis and identifying targetable pathways for high-risk endometrial cancer; a TransPORTEC initiative. Mod Pathol 2015;28:836–44.
28. León-Castillo A, Gilvazquez E, Nout R, Smit VT, McAlpine JN, McConechy M, et al. Clinicopathological and molecular characterisation of 'multiple-classifier' endometrial carcinomas. J Pathol 2020;250:312–22.
29. Workel HH, Lubbers JM, Arnold R, Prins TM, van der Vlies P, de Lange K, et al. Transcriptionally distinct CXCL13(+)CD103(+)CD8(+) T-cell population is associated with B-cell recruitment and neoantigen load in human cancer. Cancer Immunol Res 2019;7:784–96.
30. Koelzer VH, Sirinukunwattana K, Rittscher J, Mertz KD. Precision immunoprofiling by image analysis and artificial intelligence. Virchows Arch 2019;474:511–22.
31. Hastie T, Tibshirani R, Friedman J. The elements of statistical learning. Berlin (Germany): Springer-Verlag; 2009.
32. Murtagh F, Legendre P. Ward's hierarchical agglomerative clustering method: which algorithms implement Ward's Criterion? J Classification 2014;31:274–95.
33. McShane LM, Altman DG, Sauerbrei W, Taube SE, Gion M, Clark GM. Reporting recommendations for tumor marker prognostic studies (REMARK). J Nat Cancer Inst 2005;97:1180–4.
34. Creutzberg CL, van Stiphout RG, Nout RA, Lutgens LC, Jurgenliemk-Schulz IM, Jobsen JJ, et al. Nomograms for prediction of outcome with or without adjuvant radiation therapy for patients with endometrial cancer: a pooled analysis of PORTEC-1 and PORTEC-2 trials. Int J Radiot Oncol Biol Phys 2015;91:530–9.
35. Harrell FE. Regression modeling strategies: with applications to linear models, logistic regression, and survival analysis. New York: Springer; 2001.
36. Fridman WH, Pages F, Sautes-Fridman C, Galon J. The immune contexture in human tumours: impact on clinical outcome. Nat Rev Cancer 2012;12:298–306.
37. Workel HH, Komdeur FL, Wouters MC, Plat A, Klip HG, Eggink FA, et al. CD103 defines intraepithelial CD8+ PD1+ tumour-infiltrating lymphocytes of prognostic significance in endometrial adenocarcinoma. Eur J Cancer 2016;60:1–11.
38. Luke JJ, Bao R, Sweis RF, Spranger S, Gajewski TF. WNT/beta-catenin pathway activation correlates with immune exclusion across human cancers. Clin Cancer Res 2019;25:3074–83.
39. Salgado R, Denkert C, Demaria S, Sirtaine N, Klauschen F, Pruneri G, et al. The evaluation of tumor-infiltrating lymphocytes (TILs) in breast cancer: recommendations by an International TILs Working Group 2014. Ann Oncol 2015;26:259–71.
40. Clarke MA, Devesa SS, Harvey SV, Wentzensen N. Hysterectomy-corrected uterine corpus cancer incidence trends and differences in relative survival reveal racial disparities and rising rates of nonendometrioid cancers. J Clin Oncol 2019;37:1895–908.